Self-scheduled H_∞ control of autonomous vehicle in collision avoidance maneuvers

Dario Penco, Joan Davins-Valldaura, Emmanuel Godoy, Pedro Kvieska, Giorgio Valmorbida

Self-scheduled H_∞ control of autonomous vehicle in collision avoidance maneuvers

Dario Penco * **Joan Davins-Valldaura** ** **Emmanuel Godoy** *
Pedro Kvieska ** **Giorgio Valmorbida** *

* *Université Paris-Saclay, CNRS, CentraleSupélec, Laboratoire des signaux et systèmes, 91190 Gif-sur-Yvette, France.* {*dario.penco, emmanuel.godoy, giorgio.valmorbida*}*@centralesupelec.fr*
** *Groupe Renault, Technocentre, 78288 Guyancourt, France*
{*joan.davins-valldaura, pedro.kvieska*}*@renault.com*

Abstract: This article presents the development of a control law for vehicle steering, acceleration and braking in the autonomous driving context. A self-scheduled robust feedback control design strategy is proposed for the stabilization of the vehicle along a predefined reference collision avoidance maneuver. A non-linear vehicle model with tire forces saturation is developed. Its linearization along the reference trajectory leads to a Linear Parameter-Varying (LPV) model. An LPV H_∞ control law with pole placement is computed for the LPV model. Simulation results illustrate the stabilization of the vehicle along the reference trajectory.

Keywords: Autonomous Vehicles, Linear parametrically varying (LPV) methodologies, Robust control, Pole placement.

1. INTRODUCTION

Autonomous driving is widely considered a possible solution to several private transportation challenges, as for example efficiency, energy consumption and safety, as described in Litman (2020). Several *Advanced Driver-Assistance Systems* (ADAS) have been developed in the recent years, see Bengler et al. (2014). Some of these systems are able to control the vehicle under the driver supervision in specific environmental conditions. They constitute the first basic components of autonomous driving. To move towards increased levels of autonomous driving, defined in SAE (2018), less driver supervision is required. Hence safety functions have to be developed, to control the vehicle in emergency conditions. The development of methods for driving automation in collision avoidance maneuvers are of great interest for both academical and industrial communities.

The ADAS systems dealing with driving automation that are currently available on commercial vehicles mainly handle low dynamics maneuvers, i.e. maneuvers with a maximum vehicle acceleration of 0.3g. In these conditions, longitudinal and lateral vehicle dynamics can be considered uncoupled, and the tire forces behave linearly. The control of the longitudinal and lateral dynamics can hence be treated separately.

The longitudinal control architecture is usually designed hierarchically, with an higher level controller, generating the reference value for the acceleration, and a lower level controller that tracks the desired acceleration through throttle and brakes. A common solution for the higher level controller is the *Linear Proportional Integral Derivative* (PID) control law, as proposed in Persson et al. (1999), Naus et al. (2010) and Hima et al. (2011). For the lower level controller the sliding mode method can be used for engine control to deliver the required torque, as proposed in Hedrick et al. (1991) and Sei-Bum Choi and Hedrick (1995).

Lateral control is often based on the *linear bicycle model*, Rajamani (2012). There exist several solutions that propose H_2 and H_∞ control laws, as in Shimakage (2002) and Hima et al. (2011), to track lateral and yaw errors with respect to a reference trajectory.

In high dynamics maneuvers, i.e. with accelerations greater than 0.3g, other phenomena occur. The longitudinal and lateral dynamics cannot be considered decoupled. Moreover the tire forces are subject to saturation and combined longitudinal and lateral slip. As a consequence in literature a large majority of the solutions developed to control the vehicle in high dynamics conditions consider vehicle models with coupled longitudinal and lateral dynamics.

There exist several solutions based on *Model Predictive Control* (MPC) for collision avoidance maneuvers. In Falcone et al. (2007) an MPC controller is developed based on a non-linear bicycle model with both longitudinal and lateral dynamics. An alternative controller based on local linearizations of the non-linear model is also proposed to reduce the computational load. Falcone et al. (2008) and Yin et al. (2015) propose a similar controller based on a non-linear four-wheel vehicle model. In Gao et al. (2014) *tube-based* MPC is used to address also robustness criteria. The main advantage of MPC is the possibility to take into consideration the inputs and states constraints in the underlying optimization problem. It is then easy to represent actuators limits. However the framework requires a large computational load. This is a crucial point for the integration of the controller on a vehicle *Electronic Control Unit* (ECU), which for economic reasons has a limited computational capacity.

On the contrary, the *Linear Parameter-Varying* (LPV)

framework offers methods for the synthesis of controllers that do not require a large computation load; see Wu (1995), Biannic (1996), Blanchini and Miani (2015). Moreover it has already been proven effective in the vehicle dynamics control domain. In literature there exist several solutions that employ LPV controllers for *Global Chassis Control* (GCC) systems, which aim is either assist the driver by increasing vehicle stability in high dynamics conditions or improve comfort through several chassis actuators. In Fergani (2006), Gáspár et al. (2007) and Poussot-Vassal et al. (2011) different solutions for vehicle stabilisation through combinations of active steering, braking and active suspensions are proposed. They are all based on robust LPV H_∞ control law.

This paper proposes a self-scheduled LPV H_∞ controller for vehicle stabilization along a reference collision avoidance maneuver. The controller is based on a LPV model for the vehicle dynamics along the maneuver, presented by the authors in Penco et al. (2021). This LPV model is obtained from the linearization along the reference maneuver of a nonlinear model that considers the coupling between longitudinal and lateral dynamics and the tire nonlinear behavior. In particular, due to an algebraic loop introduced by the saturation function of the tires, we propose a strategy to obtain an uncertain parameter related to the slope of sector non-linearities.

The paper is organized as follows. In Section 2 the non-linear vehicle model and the procedure to obtain the LPV model are discussed. The method used for the synthesis of the controller is illustrated in Section 3. In Section 4 the results of the application of the controller in a simulation environment are shown. The conclusions and future work are discussed in Section 5.

2. PRELIMINARY RESULTS

In this section we discuss the development of a non-linear vehicle model and the procedure to obtain an LPV model. A more detailed description of the non-linear model is available in Penco et al. (2021). The difference between the model presented in Penco et al. (2021) and the model studied in this paper is the influence of the road slope and camber in the dynamical model.

2.1 Non-linear vehicle model

To obtain a model of the vehicle we consider that the two wheels of each axle have been regrouped at the center of the axle track. The vehicle degrees of freedom allow it to move on the xy plane, so it can translate along the x and y axis and rotate around the z axis. The vehicle axis are shown in Figure 1.

In Table 1 there are the model state variables and inputs. The road slope and camber angles are shown in Figure 2. Table 2 contains the forces shown in Figures 1 and 3. The forces applied on the front wheel have each a component on the x and y axis of the vehicle, that depends on δ_f. We denote the components of F_{xf} on the xy plane:

$$F_{xxf} = F_{xf}\,\cos\delta_f$$
$$F_{yxf} = F_{xf}\,\sin\delta_f.$$

The model equations of motion in the vehicle frame are:

$$m\,(\dot v - r\,u) = 2\,\big(F_{xxf} + F_{xr} - R_{xxf} - R_{xr} - F_{xyf}\big) - F_{aero} - P_x \tag{1a}$$

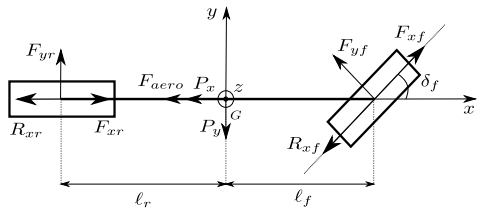

Fig. 1. Vehicle's xy plane, with the forces listed in Table 2.

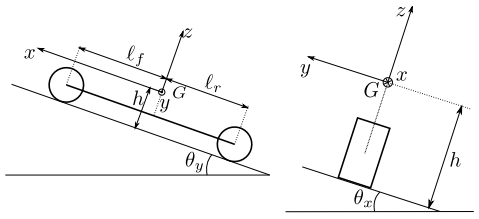

Fig. 2. Road inclination.

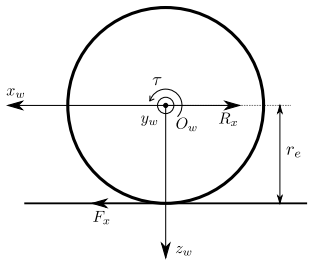

Fig. 3. Wheel's $x_w z_w$ plane.

Table 1. Model state variables and inputs

State variables		
v	[m/s]	longitudinal speed
u	[m/s]	lateral speed
r	[rad/s]	yaw rate
ω_{wf}	[rad/s]	front wheel rotational speed
ω_{wr}	[rad/s]	rear wheel rotational speed
x	[m]	absolute longitudinal position
y	[m]	absolute lateral position
ψ	[rad]	yaw angle
System's inputs		
δ_f	[deg]	front wheel steering angle
τ_{wf}	[Nm]	front wheel torque
τ_{wr}	[Nm]	rear wheel torque
θ_x	[rad]	road camber angle
θ_y	[rad]	road slope angle

Table 2. Model's forces

F_{xf}	front tire longitudinal force	F_{xr}	rear tire longitudinal force
F_{yf}	front tire lateral force	F_{yr}	rear tire lateral force
R_{xf}	front wheel rolling friction	R_{xr}	rear wheel rolling friction
F_{aero}	aerodynamic drag	P_z	weight component in z axis
P_x	weight component in x axis	P_y	weight component in y axis
N_f	front wheel normal force	N_r	rear wheel normal force

$$m\,(\dot u + r\,v) = 2\,\big(F_{yxf} - R_{yxf} + F_{yyf} + F_{yr}\big) - P_y \tag{1b}$$

$$I_{zz}\dot r = 2\,\big(F_{yxf} + F_{yyf} - R_{yxf}\big)\,\ell_f - 2\,F_{yr}\,\ell_r \tag{1c}$$

$$I_{w\,y}\,\dot\omega_{wf} = \tau_{wf} - 2\,F_{xf}\,r_e \tag{1d}$$

$$I_{w\,y}\,\dot\omega_{wr} = \tau_{wr} - 2\,F_{xr}\,r_e. \tag{1e}$$

In high dynamics maneuvers, the tires are subject to saturation and combined slip (Pacejka (2012)). It is important then to take into consideration these phenomena by using a non-linear model for the tire forces. The tire

model in Kissai et al. (2017), developed for control purposes, is a variation of the *Dugoff's model*, proposed in Dugoff et al. (1969). It is simpler and requires less parameters than other commonly used models, as the *Pacejka's magic formula*, in Bakker et al. (1987), and the *brush model*, in Svendenius (2003). We rely on this model since it allows to represent tire forces saturation and combined slip.
The longitudinal and lateral forces are linear respectively on the longitudinal and lateral slip, κ and α as

$$\hat{F}_x = c^*_\kappa(\mu, N, \alpha)\ \kappa \tag{2a}$$
$$\hat{F}_y = c^*_\alpha(\mu, N, \kappa)\ \alpha. \tag{2b}$$

Longitudinal and lateral slip κ and α are defined in Pacejka (2012). The coefficients c^*_κ and c^*_α are non-linear with respect to the α and κ respectively, the wheel normal force N and the tire-ground friction coefficient μ.
For the sake of brevity we will not discuss the tire model in details. It is however important to discuss of the tire force saturation. Here we use a circle to approximate the saturation of the tire forces as in Schuring et al. (1996), thus simplifying the more general ellipse model, discussed in Svendenius (2003). The radius of the saturation circle is given by $F_{max} = \mu N$. The logistic function, shown in Figure 4, is used to express the saturation

$$\sigma\left(\hat{F}, u, \ell\right) = \frac{u-\ell}{1+e^{-\frac{4}{u-\ell}\left(\hat{F}-\frac{u-\ell}{2}\right)}} + \ell \tag{3}$$

where u and ℓ are the upper and lower saturation bounds. The unsaturated forces $\hat{F}_x$ and $\hat{F}_y$ of (2) are the inputs of (3), the outputs are the saturated tire forces F_x and F_y.
The normal force N on the tire is present both in the coefficients c^*_κ and c^*_α and the saturation bound.
Considering the importance of N in the computation of the tire forces, a variable normal force model has then been developed. The procedure to obtain it has been discussed in Penco et al. (2021) and for brevity is not shown in this paper. The expressions of N_f and N_r depend on the longitudinal acceleration $\dot{v}$. N_f and N_r are saturated between 0 and P_z using the logistic function.
To be brief the other forces are not discussed in this paper, if needed the reader can consult Rajamani (2012).
Finally we complete the vehicle model by adding the vehicle position and orientation. Their dynamics on the inertial frame are governed by:

$$\dot{x} = v\ \cos\psi - u\ \sin\psi \tag{4a}$$
$$\dot{y} = u\ \cos\psi + v\ \sin\psi \tag{4b}$$
$$\dot{\psi} = r. \tag{4c}$$

2.2 Model linearization

The state and input vectors of the model in (1) are:

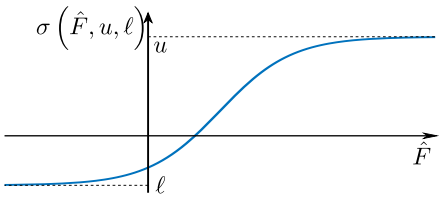

Fig. 4. Logistic function.

$$\underline{\mathbf{x}} = \begin{bmatrix} v \\ u \\ r \\ \omega_{wf} \\ \omega_{wr} \end{bmatrix} \qquad \underline{\mathbf{u}} = \begin{bmatrix} \delta_f \\ \tau_{wf} \\ \tau_{wr} \\ \theta_x \\ \theta_y \end{bmatrix}.$$

The model expressed by (1) is in implicit form $f(\dot{\underline{\mathbf{x}}}, \underline{\mathbf{x}}, \underline{\mathbf{u}}) = 0$. Due to the saturation functions used for the tire forces, it is not possible to express the model in explicit form.
We can write the model in a feedback form as in Figure 5:

$$\dot{\underline{\mathbf{x}}} = g(\underline{\mathbf{x}}, \underline{\mathbf{u}}) + B_\sigma(\underline{\mathbf{u}})\ \underline{\sigma}(\underline{\mathbf{h}}) \tag{5}$$

where:

$$\underline{\sigma}(\underline{\mathbf{h}}) = \begin{bmatrix} \sigma(h_1(\dot{\underline{\mathbf{x}}}, \underline{\mathbf{x}}, \underline{\mathbf{u}})) \\ \sigma(h_2(\dot{\underline{\mathbf{x}}}, \underline{\mathbf{x}}, \underline{\mathbf{u}})) \\ \sigma(h_3(\dot{\underline{\mathbf{x}}}, \underline{\mathbf{x}}, \underline{\mathbf{u}}, \underline{\sigma})) \\ \sigma(h_4(\dot{\underline{\mathbf{x}}}, \underline{\mathbf{x}}, \underline{\mathbf{u}}, \underline{\sigma})) \\ \sigma(h_5(\dot{\underline{\mathbf{x}}}, \underline{\mathbf{x}}, \underline{\mathbf{u}}, \underline{\sigma})) \\ \sigma(h_6(\dot{\underline{\mathbf{x}}}, \underline{\mathbf{x}}, \underline{\mathbf{u}}, \underline{\sigma})) \end{bmatrix}$$

$$\underline{\mathbf{h}}(\dot{\underline{\mathbf{x}}}, \underline{\mathbf{x}}, \underline{\mathbf{u}}, \underline{\sigma}) = \begin{bmatrix} h_1(\dot{\underline{\mathbf{x}}}, \underline{\mathbf{x}}, \underline{\mathbf{u}}) \\ h_2(\dot{\underline{\mathbf{x}}}, \underline{\mathbf{x}}, \underline{\mathbf{u}}) \\ h_3(\dot{\underline{\mathbf{x}}}, \underline{\mathbf{x}}, \underline{\mathbf{u}}, \underline{\sigma}) \\ h_4(\dot{\underline{\mathbf{x}}}, \underline{\mathbf{x}}, \underline{\mathbf{u}}, \underline{\sigma}) \\ h_5(\dot{\underline{\mathbf{x}}}, \underline{\mathbf{x}}, \underline{\mathbf{u}}, \underline{\sigma}) \\ h_6(\dot{\underline{\mathbf{x}}}, \underline{\mathbf{x}}, \underline{\mathbf{u}}, \underline{\sigma}) \end{bmatrix} = \begin{bmatrix} \hat{N}_f \\ \hat{N}_r \\ \hat{F}_{xf}\left(\sigma\left(\hat{N}_f\right)\right) \\ \hat{F}_{xr}\left(\sigma\left(\hat{N}_r\right)\right) \\ \hat{F}_{yf}\left(\sigma\left(\hat{N}_f\right)\right) \\ \hat{F}_{yr}\left(\sigma\left(\hat{N}_r\right)\right) \end{bmatrix}.$$

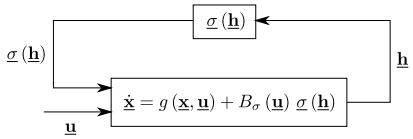

Fig. 5. Isolation of the implicit part of (1).

The vectors $\underline{\mathbf{h}}(\dot{\underline{\mathbf{x}}}, \underline{\mathbf{x}}, \underline{\mathbf{u}}, \underline{\sigma})$ and $\underline{\sigma}(\underline{\mathbf{h}})$ contain respectively the inputs and the outputs of the saturation functions. The model non-linearities due to the saturation functions have then been isolated and they result as an input of the model. The expressions of $g(\underline{\mathbf{x}}, \underline{\mathbf{u}})$ and $B_\sigma(\underline{\mathbf{u}})$ for brevity are not detailed here.
The state dynamics expressed as in (5) is then linearized along a reference trajectory $(\dot{\underline{\mathbf{x}}}_0(t), \underline{\mathbf{x}}_0(t), \underline{\mathbf{u}}_0(t), \underline{\sigma}_0(t))$, with $\underline{\sigma}_0(t) = \underline{\sigma}(\underline{\mathbf{h}}(\dot{\underline{\mathbf{x}}}_0(t), \underline{\mathbf{x}}_0(t), \underline{\mathbf{u}}_0(t)))$. For simplicity, in the following, the reference trajectory, containing both the states and the inputs, will be denoted by $\mathscr{T}(t)$.

$$\Delta\dot{\underline{\mathbf{x}}} = A(t)\Delta\underline{\mathbf{x}} + B(t)\Delta\underline{\mathbf{u}} + B_\sigma(t)\Delta\underline{\sigma}$$
$$\Delta\underline{\mathbf{h}} = C(t)\Delta\underline{\mathbf{x}} + D(t)\Delta\underline{\mathbf{u}} + D_\sigma(t)\Delta\underline{\sigma}$$

$$A(t) = \left.\frac{\partial g(\underline{\mathbf{x}}, \underline{\mathbf{u}})}{\partial \underline{\mathbf{x}}}\right|_{\mathscr{T}(t)}$$

$$B(t) = \left.\frac{\partial g(\underline{\mathbf{x}}, \underline{\mathbf{u}})}{\partial \underline{\mathbf{u}}}\right|_{\mathscr{T}(t)} + \left.\frac{\partial\left(B_\sigma(\underline{\mathbf{u}})\ \underline{\sigma}(\underline{\mathbf{h}})\right)}{\partial \underline{\mathbf{u}}}\right|_{\mathscr{T}(t)}$$

$$B_\sigma(t) = B_\sigma(\underline{\mathbf{u}})|_{\mathscr{T}(t)}$$

$$C(t) = \left.\frac{\partial \underline{\mathbf{h}}(\dot{\underline{\mathbf{x}}}, \underline{\mathbf{x}}, \underline{\mathbf{u}}, \underline{\sigma})}{\partial \dot{\underline{\mathbf{x}}}}\right|_{\mathscr{T}(t)} A(t) + \left.\frac{\partial \underline{\mathbf{h}}(\dot{\underline{\mathbf{x}}}, \underline{\mathbf{x}}, \underline{\mathbf{u}}, \underline{\sigma})}{\partial \underline{\mathbf{x}}}\right|_{\mathscr{T}(t)}$$

$$D(t) = \left.\frac{\partial \underline{\mathbf{h}}(\dot{\underline{\mathbf{x}}}, \underline{\mathbf{x}}, \underline{\mathbf{u}}, \underline{\sigma})}{\partial \dot{\underline{\mathbf{x}}}}\right|_{\mathscr{T}(t)} B(t) + \left.\frac{\partial \underline{\mathbf{h}}(\dot{\underline{\mathbf{x}}}, \underline{\mathbf{x}}, \underline{\mathbf{u}}, \underline{\sigma})}{\partial \underline{\mathbf{u}}}\right|_{\mathscr{T}(t)}$$

$$D_\sigma(t) = \left.\frac{\partial \underline{\mathbf{h}}(\dot{\underline{\mathbf{x}}}, \underline{\mathbf{x}}, \underline{\mathbf{u}}, \underline{\sigma})}{\partial \dot{\underline{\mathbf{x}}}}\right|_{\mathscr{T}(t)} B_\sigma(t) + \left.\frac{\partial \underline{\mathbf{h}}(\dot{\underline{\mathbf{x}}}, \underline{\mathbf{x}}, \underline{\mathbf{u}}, \underline{\sigma})}{\partial \underline{\sigma}}\right|_{\mathscr{T}(t)}$$

In this paper we consider the reference trajectory of Figure 6. It corresponds to a two lanes change maneuver without braking, starting at the speed of 70km/h.
The saturation functions can be approximated as sector-

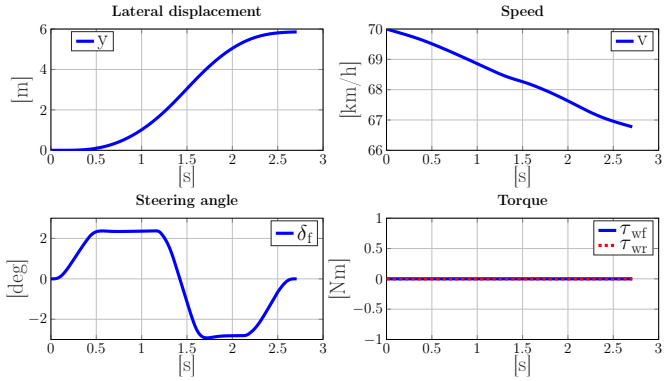

Fig. 6. Reference trajectory.

bounded non-linearities, whose slope varies according to the system working point. Figure 7 shows the slope sector for each element of $\underline{\sigma}(\underline{\mathbf{h}})$ along the reference trajectory. The wheels torques are equal to zero, hence the longitudinal tire forces and the load transfer are small and their sectors are then narrow. On the contrary the lateral tire forces magnitude in the reference trajectory includes a wider sector.

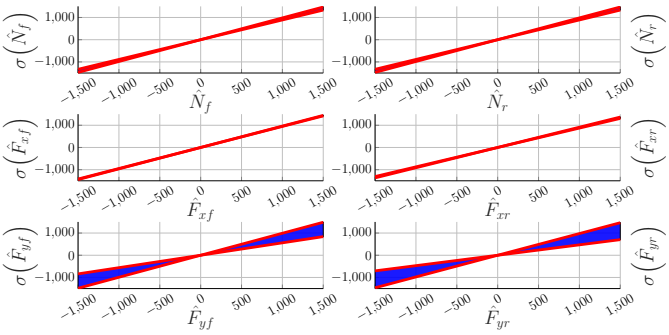

Fig. 7. Slope sector for reference trajectory of Figure 6.

We then approximate the non-linear function by a time-varying affine function as $\underline{\sigma}(\underline{\mathbf{h}}) \approx K_\sigma \underline{\mathbf{h}}$. K_σ is a time-varying diagonal matrix, with the slope of the saturation functions along the diagonal. Applying this approximation in the expression of $\Delta\underline{\mathbf{h}}$ in (6) we obtain:

$$\begin{aligned}\Delta\underline{\mathbf{h}} = &\left(I - D_\sigma(t)\, K_\sigma\right)^{-1} C(t)\Delta\underline{\mathbf{x}} \\ &+ \left(I - D_\sigma(t)\, K_\sigma\right)^{-1} D(t)\Delta\underline{\mathbf{u}}.\end{aligned}$$

Replacing this expression of $\Delta\underline{\mathbf{h}}$ in (6), the linearized state dynamics with the sector-bounded approximation of the saturation functions is:

$$\Delta\dot{\underline{\mathbf{x}}} = \widetilde{A}(t)\Delta\underline{\mathbf{x}} + \widetilde{B}(t)\Delta\underline{\mathbf{u}} \tag{7a}$$

$$\widetilde{A}(t) = A(t) + B_\sigma(t)\, K_\sigma\, \left(I - D_\sigma(t)\, K_\sigma\right)^{-1} C(t) \tag{7b}$$

$$\widetilde{B}(t) = B(t) + B_\sigma(t)\, K_\sigma\, \left(I - D_\sigma(t)\, K_\sigma\right)^{-1} D(t). \tag{7c}$$

2.3 LPV polytopic model for control synthesis

Given that the linearized model is obtained along a reference trajectory and the saturation functions are approximated by time-varying gains, the matrices $\widetilde{A}(t)$ and $\widetilde{B}(t)$ in (7b) and (7c) are time-varying.
In the following, the elements of the matrix K_σ will be considered as the average slope coefficients of the slope sector shown in Figure 7.
It is possible to consider the elements of $\widetilde{A}(t)$ and $\widetilde{B}(t)$ that vary with time as varying parameters. We call θ_i, $i = 1, \ldots, q$ these parameters. $\underline{\mathbf{p}}$ is the vector containing all the parameters. We then express the linearized model in (7) as an LPV model, with the state matrix A and the input matrix B affinely dependent on the varying parameters.
Along the reference trajectory shown in Figure 6, a total of 23 elements of $\widetilde{A}(t)$ and $\widetilde{B}(t)$ vary with time. However several of these elements have a small variation. It is possible to consider just the 6 elements of $\widetilde{A}(t)$ and $\widetilde{B}(t)$ that vary the most to constitute the vector $\underline{\mathbf{p}}$ of parameters for synthesis purposes. The range of each parameter θ_i, $i = 1, \ldots, 6$ is between a minimum $\underline{p}_i$ and a maximum $\overline{p}_i$. $\underline{p}_i$ and $\overline{p}_i$ are the minimum and maximum values of p_i along the reference trajectory $\mathscr{T}(t)$.
For the control synthesis we add the longitudinal, lateral and yaw angle errors with respect to $\mathscr{T}(t)$ to the state of the model. They are defined as:

$$\begin{aligned}x_L &= x - x_0 \\ y_L &= y - y_0 \\ \Delta\psi &= \psi - \psi_0.\end{aligned}$$

x_0, y_0 and ψ_0 are the vehicle's absolute position and attitude along the reference trajectory $\mathscr{T}(t)$.
The vehicle's position dynamics in (4a) and (4b) can be simplified neglecting the vehicle's lateral speed u, which is considerably smaller than the longitudinal speed v

$$\dot{x} = v\, \cos\psi \tag{9a}$$

$$\dot{y} = v\, \sin\psi. \tag{9b}$$

Considering that $v = v_0 + \Delta v$, $u = u_0 + \Delta u$ and $\psi = \psi_0 + \Delta\psi$ and that the $\Delta\psi$ is small along the reference trajectory, the dynamics of the error variables are:

$$\begin{aligned}\dot{x}_L &= \Delta v \\ \dot{y}_L &= \Delta v\, \psi_0 + \Delta\psi\, v_0\, \cos\psi_0 \\ \Delta\dot{\psi} &= \Delta r.\end{aligned}$$

The expressions ψ_0 and $v_0\, \cos\psi_0$ are added to $\underline{\mathbf{p}}$.
It is finally possible to define the polytopic domain $\mathcal{P}$ as the hypercube of dimension 8, each dimension being the parameter p_i, $i = 1, \ldots, 8$, between $\underline{p}_i$ and $\overline{p}_i$. The polytopic model is defined at its $N = 2^8$ vertices:

$$S_i = \begin{pmatrix} A_i & B_i \end{pmatrix} \quad i = 1, \ldots, N. \tag{11}$$

The model inside $\mathcal{P}$ is defined as:

$$S\left(\underline{\mathbf{p}}\right) = \sum_{i=1}^{N} \alpha_i \begin{pmatrix} A_i & B_i \end{pmatrix}$$

where α_i for $i = 1, \ldots, N$ are the interpolation parameters and $\sum_{i=1}^{N} \alpha_i = 1$.

3. MAIN RESULTS

A dynamic LPV H_∞ state feedback controller has been designed starting from the polytopic LPV model described in Section 2.3.
We consider the system of order n in the form:

$$\dot{\underline{\mathbf{x}}} = A_i\, \underline{\mathbf{x}} + B_{1i}\, \underline{\mathbf{w}} + B_2\, \underline{\mathbf{u}} \tag{12a}$$

$$\underline{\mathbf{z}} = C_{1i}\, \underline{\mathbf{x}} + D_{11i}\, \underline{\mathbf{w}} + D_{12}\, \underline{\mathbf{u}} \tag{12b}$$

$$\underline{\mathbf{y}} = C_2\, \underline{\mathbf{x}} + D_{21}\, \underline{\mathbf{w}} \tag{12c}$$

for $i = 1, \ldots, N$, where $\underline{\mathbf{y}}$ is the controller input, $\underline{\mathbf{z}}$ contains the controlled variables, $\underline{\mathbf{w}}$ the exogenous inputs and $\underline{\mathbf{u}}$ the control inputs. The system in the polytopic domain $\mathcal{P}$ is then expressed with respect to the N vertices:

$$S\left(\underline{\mathbf{p}}\right) = \sum_{i=1}^{N} \alpha_i \begin{pmatrix} A_i & B_{1i} & B_2 \\ C_{1i} & D_{11i} & D_{12} \\ C_2 & D_{21} & 0 \end{pmatrix} \tag{13}$$

where α_i for $i = 1, \ldots, N$ are the interpolation coefficients. In this article, the solution proposed in Chilali and Gahinet (1996) is used for the synthesis of the LPV H_∞ controller. This method allows to specify limits to the dynamics of the closed loop. This is obtained by computing a full-order LPV controller $K\left(\underline{\mathbf{p}}\right)$ that forces the closed loop eigenvalues into some LMI region for all admissible values of (13) in $\mathcal{P}$.
An LMI region $\mathcal{D} = \left\{z \in \mathbb{C} : \quad L + zM + \bar{z}M^T < 0\right\}$ of order s is a subset of the complex plane, with $L = L^T \in \mathbb{R}^{s\times s}$ and $M \in \mathbb{R}^{s\times s}$.
Given a polytopic plant (12), an LMI region $\mathcal{D}$ and the H_∞ performance $\gamma > 0$, we search an LPV controller such that: (A) the closed loop poles for all admissible values of (13) in $\mathcal{P}$ are in $\mathcal{D}$; (B) the $\mathcal{L}_2$-norm of the input/output mapping from $\underline{\mathbf{w}}$ to $\underline{\mathbf{z}}$ is bounded by γ. It exists if there exist two symmetric matrices R, $S \in \mathbb{R}^{n\times n}$ and matrices $\mathcal{A}_K$, $\mathcal{B}_K$, $\mathcal{C}_K$ and D_K such that:

$$\begin{pmatrix} R & I \\ I & S \end{pmatrix} > 0$$

$$\begin{bmatrix} \Psi_{11} & \Psi_{21}^T \\ \Psi_{21} & \Psi_{22} \end{bmatrix} < 0$$

$$L \otimes \begin{pmatrix} R & I \\ I & S \end{pmatrix} + M \otimes \Phi + M^T \otimes \Phi^T < 0$$

where, for $i = 1, \ldots, N$

$$\Phi = \begin{bmatrix} A_iR + B_2\mathcal{C}_K & A_i + B_2D_KC_2 \\ \mathcal{A}_K & SA_i + \mathcal{B}_KC_2 \end{bmatrix}$$

$$\Psi_{11} = \begin{bmatrix} A_iR + RA_i^T + B_2\mathcal{C}_K + \mathcal{C}_K^TB_2^T & B_{1i} + B_2D_KD_{21} \\ \left(B_{1i} + B_2D_KD_{21}\right)^T & -\gamma I \end{bmatrix}$$

$$\Psi_{21} = \begin{bmatrix} \mathcal{A}_K + \left(A_i + B_2D_KC_2\right)^T & SB_{1i} + \mathcal{B}_KD_{21} \\ C_{1i}R + D_{12}\mathcal{C}_K & D_{11i} + D_{12}D_KD_{21} \end{bmatrix}$$

$$\Psi_{22} = \begin{bmatrix} A_i^TS + SA_i + \mathcal{B}_KC_2 + C_2^T\mathcal{B}_K^T & \left(C_{1i} + D_{12}D_KC_2\right)^T \\ C_{1i} + D_{12}D_KC_2 & -\gamma I \end{bmatrix}$$

We compute any square matrices M and N such that $MN^T = I - RS$. Solving the system of equation:

$$\begin{aligned} \mathcal{B}_K &= NB_{Ki} + SB_2D_K \\ \mathcal{C}_K &= C_{Ki}M^T + D_KC_2R \\ \mathcal{A}_K &= NA_{Ki}M^T + NB_{Ki}C_2R + SB_2C_{Ki}M^T \\ &\quad + S\left(A_i + B_2D_KC_2\right)R \end{aligned}$$

for $i = 1, \ldots, N$, for B_{Ki}, C_{Ki} and A_{Ki} we find the controller matrices at the vertices of the polytopic domain $\mathcal{P}$. The full-order LPV H_∞ controller is:

$$K\left(\underline{\mathbf{p}}\right) = \sum_{i=1}^{N} \alpha_i \begin{pmatrix} A_{Ki} & B_{Ki} \\ C_{Ki} & D_K \end{pmatrix}.$$

For the control synthesis an LMI region has been used. It guarantees that the closed loop eigenvalues for all admissible values in $\mathcal{P}$ are between $\underline{\lambda} = -8500$ and $\overline{\lambda} = -1.8$, to bound slow and fast dynamics, and $\theta = 1.12$rad, to have a minimum damping ratio $\zeta > 0.9$.
To bound the bandwidth of the control signals a diagonal weighting function W_u as been used, where the elements on the diagonal are $W_{u1}(s) = \frac{100s+31.57}{s+315.7}$ and $W_{u2}(s) = W_{u3}(s) = \frac{100s+315.7}{s+3157}$. The control architecture is represented in Figure 8.

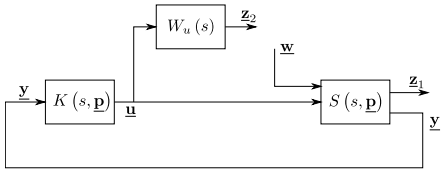

Fig. 8. Control architecture.

We define $\underline{\mathbf{z}} = \left[\underline{\mathbf{z}}_1, \underline{\mathbf{z}}_2\right]^T$, $\underline{\mathbf{y}} = \underline{\mathbf{x}}$ and:

$$\underline{\mathbf{x}} = \begin{bmatrix} \Delta v \\ \Delta u \\ \Delta r \\ \Delta\omega_{wf} \\ \Delta\omega_{wr} \\ x_L \\ y_L \\ \Delta\psi \end{bmatrix} \quad \underline{\mathbf{w}} = \begin{bmatrix} \Delta\theta_x \\ \Delta\theta_x \end{bmatrix} \quad \underline{\mathbf{u}} = \begin{bmatrix} \Delta\delta_f \\ \Delta\tau_{wf} \\ \Delta\tau_{wr} \end{bmatrix} \underline{\mathbf{z}}_1 = \begin{bmatrix} x_L \\ y_L \\ \Delta\psi \end{bmatrix}. \tag{17}$$

The matrix B_{1i} and B_2 are obtained from B_i in (11), given the definitions of $\underline{\mathbf{w}}$ and $\underline{\mathbf{u}}$ in (17).

4. NUMERICAL RESULTS

In this Section some numerical results of the controller are shown. The controller has been tested on MATLAB/Simulink on the non-linear bicycle model described in Section 2.1. The trajectory considered is the reference trajectory shown in Section 2.2, Figure 6.
Several simulations have been carried out, with a set of different initial conditions for Δv and Δu, to establish empirically the region of initial conditions for which the controller is able to stabilize the system and converge to the reference trajectory. Figure 9 shows the empirical region of attraction of the controller for non-zero initial conditions for the variables Δv and Δu. The capacity of the controller to stabilize the system and bring back the vehicle along the reference trajectory is limited for $-5.2\text{m/s} \lesssim \Delta v\,(0) \lesssim 4.3\text{m/s}$ and $-5\text{m/s} \lesssim \Delta u\,(0) \lesssim 8.4\text{m/s}$.

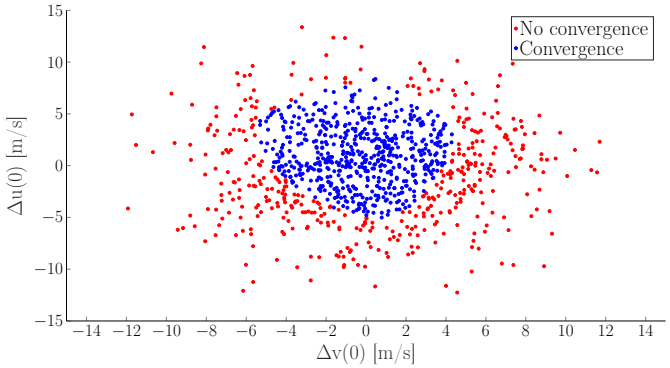

Fig. 9. Empirical region of attraction for Δv and Δu.

A case with initial conditions of $\Delta v\,(0) = 3\text{m/s}$, $\Delta u\,(0) = 2\text{m/s}$ and $\Delta r\,(0) = 15\text{deg/s}$ is simulated and shown in detail. Figure 10 shows the commands computed by the controller, the vehicle's position and attitude error and the vehicle overall longitudinal and lateral accelerations. Due to the large initial conditions, the position errors are initially large, but they eventually converge to zero. Indeed the vehicle acceleration belong to the high dynamics category.

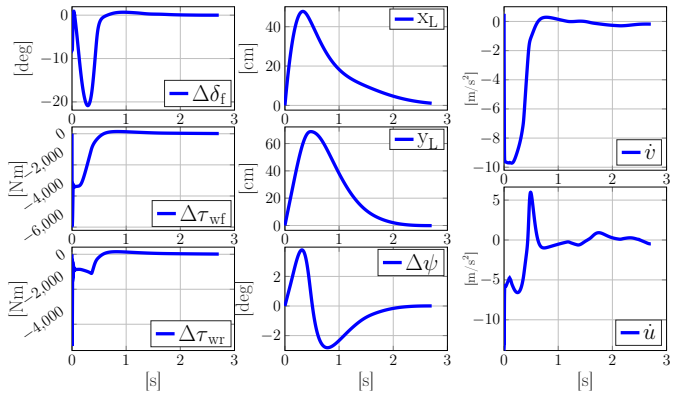

Fig. 10. Simulation results.

5. CONCLUSION AND PERSPECTIVES

The LPV model discussed in Section 2 had already been used by the authors for the synthesis of a static state feedback controller in Penco et al. (2021). The results of Section 4 show that the LPV H_∞ dynamic controller developed in Section 3, compared to the static controller developed in Penco et al. (2021), considerably enlarges the range of initial conditions for which the controller is able to stabilize the system along the reference trajectory. Moreover this has been obtained considering also the road inclination as system perturbation. A more thorough methodology to estimate the region of attraction of the closed-loop systems, without simulations, will be proposed by considering sector inequalities associated to the saturation function.

REFERENCES

Bakker, E., Nyborg, L., and Pacejka, H.B. (1987). Tyre modelling for use in vehicle dynamics studies. In *SAE Technical Paper*.

Bengler, K., Dietmayer, K., Farber, B., Maurer, M., Stiller, C., and Winner, H. (2014). Three Decades of Driver Assistance Systems: Review and Future Perspectives. *IEEE Intelligent Transp. Sys. Mag.*, 6, 6–22.

Biannic, J. (1996). *Commande robuste des systèmes a paramètres variables. Applications en aéronautique.* Ph.D. thesis, Ecole nationale supérieure de l'aéronautique et de l'espace.

Blanchini, F. and Miani, S. (2015). *Set-Theoretic Methods in Control.* Springer International Publishing.

Chilali, M. and Gahinet, P. (1996). H_∞ Design with Pole Placement Constraints: an LMI Approach. *IEEE Transactions on Automatic Control*, 41, 358–367.

Dugoff, H., Fancher, P., and Segel, L. (1969). Tire performance characteristics affecting vehicle response to steering and braking control input. *Highway Safety Research Institute of Science and Technology.*

Falcone, P., Borrelli, F., Asgari, J., Tseng, H.E., and Hrovat, D. (2007). Predictive active steering control for autonomous vehicle systems. *IEEE Transactions on Control Systems Technology*, 15, 566–580.

Falcone, P., Tseng, H.E., Borrelli, F., Asgari, J., and Hrovat, D. (2008). MPC-based yaw and lateral stabilisation via active front steering and braking. *Vehicle System Dynamics*, 46, 611–628.

Fergani, S. (2006). *Robust multivariable control for vehicle dynamics.* Ph.D. thesis, Université de Grenoble.

Gao, Y., Gray, A., Tseng, H.E., and Borrelli, F. (2014). A tube-based robust nonlinear predictive control approach to semiautonomous ground vehicles. *Vehicle System Dynamics*, 52, 802–823.

Gáspár, P., Szabó, Z., Bokor, J., Poussot-Vassal, C., Sename, O., and Dugard, L. (2007). Towards global chassis control by integrating the brake and suspention system. *IFAC Proceedings Volumes*, 40, 563–570.

Hedrick, J.K., McMahon, D., Narendran, V., and Swaroop, D. (1991). Longitudinal Vehicle Controller Design for IVHS Systems. In *1991 American Control Conference*, 3107–3112. Boston, MA, USA.

Hima, S., Lusseti, B., Vanholme, B., Glaser, S., and Mammar, S. (2011). Trajectory tracking for highly automated passenger vehicles. *IFAC Proceedings Vol.*, 44, 12958–12963.

Kissai, M., Monsuez, B., Tapus, A., and Martinez, D. (2017). A new linear tire model with varying parameters. In *2017 2nd IEEE International Conf. on Intelligent Transp. Engineering (ICITE)*, 108–115. Singapore.

Litman, T. (2020). Autonomous Vehicle Implementation Predictions: Implications for Transport Planning.

Naus, G.J.L., Vugts, R.P.A., Ploeg, J., van de Molengraft, M.J.G., and Steinbuch, M. (2010). String-stable CACC design and experimental validation: A frequency-domain approach. *IEEE Trans. on Veh. Tech.*, 59, 4268–4279.

Pacejka, H.B. (2012). *Tyre and vehicle dynamics.* Elsevier.

Penco, D., Davins-Valldaura, J., Godoy, E., Kvieska, P., and Valmorbida, G. (2021). Control for autonomous vehicles in high dynamics maneuvers : LPV modeling and static feedback controller. In *Conference on Control Technology and Applications (CCTA).* San Diego, USA.

Persson, M., Botling, F., Hesslow, E., and Johansson, R. (1999). Stop and go controller for adaptive cruise control. In *Proceedings of the 1999 IEEE International Conference on Control Applications*, 1692–1697 vol. 2. Kohala Coast, HI, USA.

Poussot-Vassal, C., Sename, O., Dugard, L., and Savaresi, S.M. (2011). Vehicle dynamic stability improvements through gain-scheduled steering and braking control. *Vehicle System Dynamics*, 49, 1597–1621.

Rajamani, R. (2012). *Vehicle dynamics and control.* Springer US.

SAE (2018). Taxonomy and Definitions for Terms Related to Driving Automation Sys. for On-Road Motor Vehicles.

Schuring, D.J., Pelz, W., and Pottinger, M.G. (1996). A model for combined tire cornering and braking forces. In *SAE Technical Paper.*

Sei-Bum Choi and Hedrick, J.K. (1995). Vehicle longitudinal control using an adaptive observer for automated highway systems. In *Proceedings of 1995 American Control Conf. - ACC'95*, 3106–3110. Seattle, WA, USA.

Shimakage, M. (2002). Design of lane-keeping control with steering torque input. *JSAE Review*, 23, 317–323.

Svendenius, J. (2003). *Tire Modeling and Friction Estimation.* Ph.D. thesis, Lund University.

Wu, F. (1995). *Control of Linear Parameter Varying Systems.* Ph.D. thesis, Univ. of California at Berkeley.

Yin, G., Li, J., Jin, X., Bian, C., and Chen, N. (2015). Integration of motion planning and model-predictive-control-based control system for autonomous electric vehicles. *Transport*, 30, 353–360.